Article

# Characterization of Planar Lead Halide Perovskite Solar Cells by Impedance Spectroscopy, Open-Circuit Photovoltage Decay, and Intensity-Modulated Photovoltage/Photocurrent Spectroscopy

Adam Pockett,[†] Giles E. Eperon,[‡] Timo Peltola,[§] Henry J. Snaith,[‡] Alison Walker,[§] Laurence M. Peter,*[,†] and Petra J. Cameron*[,†]

[†]Department of Chemistry and [§]Department of Physics, University of Bath, Bath BA2 7AY, United Kingdom
[‡]Clarendon Laboratory, Parks Road, Oxford OX1 3PU, United Kingdom

**S** Supporting Information

**ABSTRACT:** Thin film lead halide perovskite cells, where the perovskite layer is deposited directly onto a flat titania blocking layer, have reached AM 1.5 efficiencies of over 15%,[1] showing that the mesoporous scaffold used in early types of perovskite solar cells is not essential. We used a variety of techniques to gain a better understanding of thin film perovskite cells prepared by a solution-based method. Twelve cells were studied, which showed AM 1.5 efficiencies of ~11%. The properties of the cells were investigated using impedance spectroscopy, intensity-modulated photovoltage spectroscopy (IMVS), intensity-modulated photocurrent spectroscopy (IMPS), and open-circuit photovoltage decay (OCVD). Despite the fact that all 12 cells were prepared at the same time under nominally identical conditions, their behavior fell into two distinct groups. One half of the cells exhibited ideality factors of $m \approx 2.5$, and the other half showed ideality factors of $m \approx 5$. Impedance spectroscopy carried out under illumination at open circuit for a range of intensities showed that the cell capacitance was dominated by the geometric capacitance of the perovskite layer rather than the chemical or diffusion capacitance due to photogenerated carriers. The voltage dependence of the recombination resistance gave ideality factors similar to those derived from the intensity dependence of the open-circuit voltage. The IMVS time constant was determined by the product of the geometric capacitance and the recombination resistance. The two types of cells gave very different OCVD responses. The cells with $m \approx 2.5$ showed a persistent photovoltage effect that was absent in the case of the cells with higher ideality factors. The IMPS responses provide evidence of minor efficiency losses by recombination under short-circuit conditions.
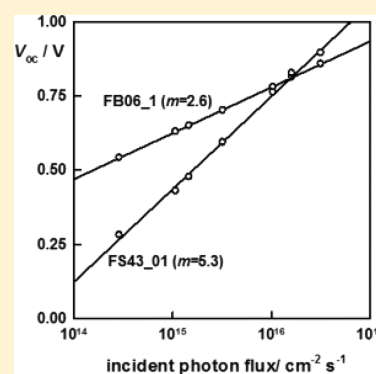
## INTRODUCTION

The rapid development of organometal halide perovskite solar cells[2−5] based on $CH_3NH_3PbI_3$ and its analogs continues to set new records in terms of efficiency[6] that already far exceed those for dye-sensitized solar cells or organic photovoltaics. The high open-circuit voltages and high external quantum efficiencies point to unusually slow recombination of electrons and holes in the perovskite absorber layer, with second-order rate constants for uncontacted thin films reported to be four orders lower than the Langevin limit for bimolecular recombination.[7] The reasons for such slow recombination are currently a central topic of discussion,[8−10] and it has been suggested that the formation of ferroelectric domains may lead to spatial separation of electrons and holes.[11,12] It has also been reported that the lead halide perovskites exhibit a photoinduced giant dielectric effect (GDE) with a relaxation time constant in the region of seconds.[13] The high open-circuit voltages (in excess of 1 V) also indicate that the built-in voltage of the junction must be unusually high (>1 V) relative to the band gap of the perovskite (ca. 1.5 eV). Reported band alignments in the $TiO_2$|perovskite| spiro-OMeTAD structure[14] suggest that the built-in voltage in the thin perovskite layer could exceed 1.2 V.

In principle, electron−hole recombination can occur either in the bulk of the perovskite or at the contacts, which are made using materials that are selective for extraction of electrons (e.g., $TiO_2$) or holes (e.g., spiro-OMeTAD). A number of methods have been used to study electron−hole recombination including transient microwave[9,15,16] and terahertz[9,16,17] measurements, photoluminescence,[18] transient absorbance,[7,18] EBIC,[19] photovoltage and photocurrent transients,[20] impedance,[21−24] and open-circuit voltage decay.[25] Many of these studies have characterized the properties of perovskite cells fabricated using mesoporous oxide substrates of either $TiO_2$ or $Al_2O_3$. However, interest is increasingly being focused on planar junction perovskite cells that appear in many instances to operate as p−i−n devices.[19] For this reason we chose to characterize batches of planar perovskite cells using a range of complementary techniques, namely, impedance, intensity-modulated photovoltage spectroscopy (IMVS), intensity-modulated photocurrent spectroscopy (IMPS), open-circuit

photovoltage decay (OCPVD), and steady-state photovoltage measurements as a function of light intensity. The use of these six techniques on a large number of cells allowed us to assess the consistency of the conclusions.

The series of 12 planar perovskite devices could be divided clearly into two groups on the basis of the intensity dependences of the open-circuit voltage, which corresponded to diode ideality factors that clustered either around ~2.5 or around ~5.0. The high-frequency impedance and intensity-modulated photovoltage (IMVS) responses of the cells were modeled satisfactorily using a simple lumped RC circuit. At low frequencies an additional feature was observed which Juárez-Pérez et al.[13] attributed to a photoinduced giant dielectric effect. The influence of the GDE on the low-frequency impedance response has been modeled by Bisquert et al.,[26] but in this paper the low-frequency feature has not been included in modeling. Substantial information about the cell was extracted using the simple lumped model at mid and high frequencies, and we are currently measuring and modeling the low-frequency feature separately. The results obtained at open circuit by impedance and IMVS are in good agreement, both indicating that for open-circuit voltages below 0.9 V, the geometric capacitance associated with charge in the contacting phases ($TiO_2$ and spiro-OMeTAD) is larger than the chemical (or diffusion) capacitance associated with the buildup of electrons and holes in the perovskite absorber, even at the highest light intensities used here (equivalent to 0.1 Sun). The voltage dependence of the recombination resistance gave nonideality factors close to those derived from the intensity dependence of the open-circuit voltage. OCVD also reveals that some cells exhibit a persistent photovoltage that extends the decay time into the region of seconds when the voltage falls below 0.4 V.

## ■ EXPERIMENTAL SECTION

**Perovskite Precursor Preparation.** Methylamine iodide (MAI) was prepared by reacting methylamine, 33 wt % in ethanol (Sigma-Aldrich), with hydroiodic acid (HI), 57 wt % in water (Sigma-Aldrich), at room temperature. HI was added dropwise while stirring. Upon drying at 100 °C, a white powder was formed, which was washed with ethanol and dried overnight in a vacuum oven before use.

To form the nonstoichiometric $CH_3NH_3PbI_{3-x}Cl_x$ precursor solution, methylammonium iodide and lead(II) chloride (98%, Sigma-Aldrich) were dissolved in anhydrous N,N-dimethylformamide (DMF) at a 3:1 molar ratio of MAI to $PbCl_2$, with final concentrations of 0.88 M lead chloride and 2.64 M methylammonium iodide. This solution is stored under a dry nitrogen atmosphere.

**Substrate Preparation.** Devices were fabricated on fluorine-doped tin oxide (FTO) coated glass (Pilkington, 7 Ω □$^{-1}$). To prevent shunting upon contact with measurement pins, FTO was removed from regions under the anode contact by etching with 2 M HCl and zinc powder. Substrates were then cleaned sequentially in 2% Hellmanex detergent, acetone, propan-2-ol, and oxygen plasma. A hole-blocking layer of compact $TiO_2$ was deposited by spin coating a mildly acidic solution of titanium isopropoxide in anhydrous ethanol (350 μL in 5 mL of ethanol with 0.013 M HCl) and annealed at 500 °C for 30 min. Spin coating was carried out at 2000 rpm for 60 s.

**Perovskite Solar Cell Fabrication.** A total of 12 cells was fabricated in groups of 3 cells on one substrate, each with a pixel area of 0.15 cm². To form the perovskite layer, the nonstoichiometric precursor was spin coated on the substrate in a nitrogen-filled glovebox at 2000 rpm for 45 s. After spin coating, the films were left to dry at room temperature in the glovebox for 30 min to allow slow solvent evaporation. They were then annealed on a hot plate in the glovebox at 90 °C for 180 min and subsequently at 120 °C for 15 min.

A hole-transporting layer was then deposited via spin coating a 0.79 M solution of 2,2′,7,7′-tetrakis(N,N-di-p-methoxyphenylamine)-9,9′-spirobifluorene (spiro-OMeTAD) in chlorobenzene, with additives of lithium bis(trifluoromethanesulfonyl)imide (0.0184 M) and 4-tert-butylpyridine (0.0659 M). Spin coating was carried out at 2000 rpm for 45 s. Devices were then left overnight in air for the spiro-OMeTAD to dope via oxidation. Finally, gold electrodes were thermally evaporated under a vacuum of ~$10^{-6}$ Torr at a rate of ~0.1 nm s$^{-1}$ to complete the devices.

**Solar Cell Characterization.** The current density–voltage (J–V) curves were measured (2400 Series SourceMeter, Keithley Instruments) under simulated AM 1.5 sunlight at 100 mW cm$^{-2}$ irradiance generated by an Abet Class AAB sun 2000 simulator, with the intensity calibrated with an NREL calibrated KG5-filtered Si reference cell. The mismatch factor was calculated to be 1.2% between 400 and 1100 nm. The solar cells were masked with a metal aperture to define the active area, typically 0.0625 cm$^{-2}$, and measured in a light-tight sample holder to minimize any edge effects.

The cells were stored in a nitrogen glovebox between measurements to minimize degradation. Open-circuit voltages were measured as a function of light intensity using a 625 nm light-emitting diode (LED) (Thorlabs MRLED). The incident photon flux was controlled using neutral density filters (Edmund Optics) and measured using a calibrated silicon photodiode (Newport 818-SL with OD3 neutral density filter). All modulated techniques were also carried out with illumination from a 625 nm LED where appropriate (Thorlabs MRLED). Impedance measurements for different illumination intensities were made at the corresponding open-circuit voltage using an Autolab PGSTAT30. Impedance measurements were also made in the dark as a function of applied voltage. Impedance data were fitted using ZView software (Scribner Associates). IMVS and IMPS measurements were made using a Solartron 1260 frequency response analyzer (FRA) combined with a Thorlabs DC2100 controller (bandwidth 100 kHz) driven by the dc and sine wave output of the FRA. The modulation depth was set to be 10% of the dc level. The illumination intensity was varied using calibrated neutral density filters. To ensure long-term stability, cells were illuminated with a single wavelength at intensities of 0.1 Sun and lower. By measuring trends with respect to illumination intensity we were able to derive significant amounts of information on cell behavior. In the environment solar cells need to operate at illumination intensities below 1 Sun; therefore, tests of cell performance at 0.1 Sun can still be considered as the working environment for a cell. To correct for attenuation and phase lag in the modulated light output at higher frequencies, a glass microscope slide was used as a beam splitter enabling provision of a reference signal for the frequency response analyzer from a fast p–i–n photodiode. For IMPS, the cell current was measured using a current amplifier (Femto DLPCA-200). A high-impedance (>$10^{12}$ ohm) voltage follower was used for IMVS. The bandwidth of the system was checked using a fast p–i–n photodiode in place

of the solar cell. OCVD measurements were made using step function illumination of the cells (625 nm LED; on period 60 s). The voltage decay after switching the light off was measured using the high-impedance voltage follower amplifier and a digital storage oscilloscope. Care was taken to totally exclude stray light.

## ■ THEORY

**Diode Ideality Factor.** The diode ideality factor, $n$, is normally defined in terms of the Shockley diode equation, which describes the dependence of the diode current density, $j$, on the applied voltage $V$. Here, $j_{sat}$ is the reverse saturation current

$$j = j_{sat}\left(e^{qV/nk_BT} - 1\right) \tag{1}$$

In theory, $n$ can take different values between 1 and 3, depending on the recombination mechanism[27] (Hall Shockley Read, Sah Noyce Shockley, Auger, etc.), although in some cases anomalously high experimental values of $n$ may point to the existence of several junctions in a device.[28] Here, we are mainly concerned with the behavior of perovskite cells under illumination, and so we define a diode ideality factor $m$ using the intensity dependence of the open-circuit voltage, which takes the form

$$\frac{\partial V_{oc}}{\partial \ln I_0} = \frac{mk_BT}{q} \tag{2}$$

The ideality factors $n$ and $m$ are not identical for perovskite solar cells since the dark and light current voltage plots cross at forward bias (see Supporting Information).

**Impedance.** A simple equivalent circuit for a planar thin film p−i−n solar cell is shown in Figure 1. Here, the
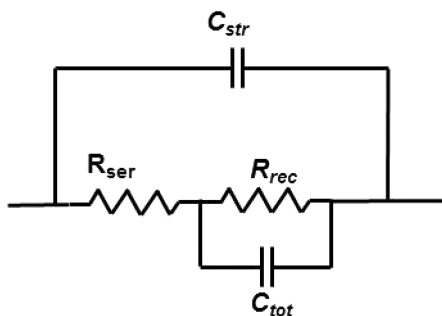


**Figure 1.** Equivalent circuit of a thin film solar cell with elements representing the recombination resistance, $R_{rec}$, cell capacitance, $C_{tot}$, series resistance, $R_{ser}$, and the stray capacitance $C_{str}$.

capacitance $C_{total}$ reflects the *overall* charge storage in the device. This is the sum of (a) the charge in the contacts (related linearly to the voltage by the geometric or junction capacitance, $C_{geo}$) and (b) the charge associated with photogenerated electrons and holes in the perovskite layer (usually related exponentially to the voltage by the chemical capacitance, $C_\mu$). The relationship between $C_{geo}$ and $C_\mu$ is discussed in more detail in the main text and also in the Supporting Information.

Recombination is represented by the voltage-dependent recombination resistance, $R_{rec}$, defined by

$$R_{rec} = \left(\frac{\partial V}{\partial j_{rec}}\right) \tag{3}$$

where $j_{rec}$ is the recombination current density. Generally, the variation of the recombination resistance with voltage is related to the ideality factor $m$ by

$$\frac{\partial \log R_{rec}}{\partial V} = -\frac{q}{2.303mk_BT} \tag{4}$$

$R_{ser}$ is the series resistance of the cell, which in the present case is largely associated with the FTO substrate. $C_{total}$ represents the total capacitance of the cell, $C_{geo} + C_\mu$. If necessary, it can be replaced by constant phase shift elements (CPE) to reflect effects such as those arising from heterogeneity (see Supporting Information for a discussion of CPE behavior).[29,30] In the case where $C_{total}$ is dominated by the buildup of photogenerated charge (as in the DSC and in silicon p−n devices),[31,32] the recombination lifetime is given by the product of the chemical capacitance $C_\mu$ and the recombination resistance $R_{rec}$. In the case where the geometric capacitance, $C_{geo}$, dominates the recombination lifetime is not obtained and the time constant for the process is $R_{rec}C_{geo}$.

The circuit shown in Figure 1 neglects complications that arise in the case of perovskite cells from low-frequency effects. These have been discussed recently by Bisquert et al.,[26] who attribute the low-frequency response to the GDE. Discussion of the low-frequency response of the planar cells is deferred to a forthcoming paper. In general, the circuit model in Figure 1 gives a satisfactory fit of the impedance data for the planar perovskite cells at frequencies above 100 Hz. The low-frequency feature only becomes an issue at low light intensities (low open-circuit voltages), where the $RC$ time constant of the solar cell becomes comparable with the time constant for the process.[29]

The circuit in Figure 1 differs from the transmission line model that has been used for mesoporous perovskite solar cells.[10,21] As shown below, the planar perovskite cells investigated here do not show transmission line behavior even in the highest frequency part of the impedance responses, indicating that transport of charge carriers by drift/diffusion is very fast in the thin (600 nm) perovskite absorber layer.

## ■ IMVS AND OCVD

Intensity-modulated photovoltage spectroscopy (IMVS) has been widely used to study recombination in dye-sensitized solar cells (DSC). It has also been used to investigate mesostructured perovskite cells.[33−35] To the best of our knowledge, this is the first time IMVS has been used to characterize *planar* perovskite cells. The method involves using a small sinusoidal modulation of the illumination intensity to perturb the Fermi level splitting around a steady state at open circuit. Generally, the IMVS response is a semicircle with a characteristic radial frequency at its maximum that is the inverse of the photovoltage decay time constant, $\tau_{IMVS}$. In the case where the effects of the geometric or junction capacitance can be neglected, $\tau_{IMVS}$ is given by the product of the recombination resistance and the chemical capacitance, which corresponds to the ambipolar carrier lifetime. However, in the case where $C_{geo}$ is dominant, we expect $\tau_{IMVS}$ to be determined by the product $R_{rec}C_{geo}$.

For open-circuit photovoltage decay (OCVD) measurements, the cell is illuminated at open circuit to establish a photostationary state. The light is then switched off, and the decay in $V_{oc}$ is monitored as a function of time. The photovoltage decay lifetime, $\tau_{OCVD}$, is then obtained using eq 5 (see Supporting Information).

$$\tau_{OCVD} = -\frac{2k_B T}{q}\left(\frac{dV_{OC}}{dt}\right)^{-1} - \frac{dV_{OC}}{dt}\left(\frac{d^2 V_{OC}}{dt^2}\right)^{-1} \tag{5}$$

Equation 5 is derived using an approach similar to that of Zaban et al.[36] but for the two carrier case where the excess carrier densities are higher than the doping density of the material (see Supporting Information). The second term in eq 5 is often omitted, and a satisfactory approximation of the lifetime can be obtained by the first term (see ref 31 for more details).

If the chemical capacitance of the cell is larger than the geometric capacitance obtained from eq 5, the decay lifetime corresponds to the ambipolar carrier lifetime. However, in the case where the geometric/junction capacitance dominates, we expect $\tau_{OCVD}$ to correspond to the $RC$ time constant $R_{rec}C_{geo}$.

## ■ IMPS

In cases where carrier transport is slow, the IMPS response can be used to measure the delay in collecting carriers at the contacts. IMPS has been used extensively to study trap-limited electron transport in dye-sensitized solar cells.[37,38] It has also been used to study mesostructured perovskite solar cells.[33] However, in the case of normal p–n or p–i–n solar cells without deep trap states, carrier separation is so fast that it is much more difficult to measure by IMPS. The high-frequency IMPS response is dominated in this case by the attenuation arising from the time constant of the solar cell, which corresponds to $R_{ser}C_{total}$ in Figure 1. By contrast, in the case of mesostructured perovskite solar cells, IMPS may give both the RC time constant and a time constant due to electron transport in the mesoporous titania scaffold. IMPS has also been used to characterize charge transfer and recombination in semiconductor–electrolyte contacts.[38,39] In this case, the modulated illumination generates a flux of minority carriers into the surface (e.g., at the semiconductor–solution interface). Once there, the carriers either can be involved in a charge transfer reaction or may combine with majority carriers. The relaxation of the minority carrier concentration at the surface by charge transfer and recombination gives rise to a semicircle in the complex plane IMPS plot with a radial frequency at the maximum that is equal to the inverse of the relaxation lifetime $\tau_{IMPS}^{-1} = k_{trans} + k_{rec}$. The normalized low-frequency intercept of the IMPS plot corresponds to the dc response, and it depends on the fraction of the minority carriers that make it across the interface. This *charge transfer efficiency*, $\eta_{trans}$, is given simply by the ratio $k_{trans}/(k_{trans} + k_{rec})$.[39,40] Here, $k_{trans}$ and $k_{rec}$ are first-order (or pseud- first-order) rate constants for charge transfer and recombination at short circuit, respectively.

## ■ RESULTS AND DISCUSSION

**Cell Efficiencies.** Representative IV curves (Figures S1 and S2) and a summary of the efficiencies of all the cells used in this study are given in the Supporting Information. Five devices were studied, each of which contained three pixels, making a total of 15 solar cells. The cells showed an average efficiency of 11.05% at 1 Sun and AM1.5 with a standard deviation of 1.02% (number of samples, $n = 14$). The two cells presented in most detail below had efficiencies of 11.98% (FS43_1) and 9.60% (FB06_1). One of the pixels gave an anomalously low efficiency and was disregarded, two further pixels degraded during transport, and the data from them was also not included in the study.

**Intensity Dependence of $V_{oc}$.** All of the cells were made at the same time using identical techniques and annealed together on the same hot plate. Figure 2 illustrates the two
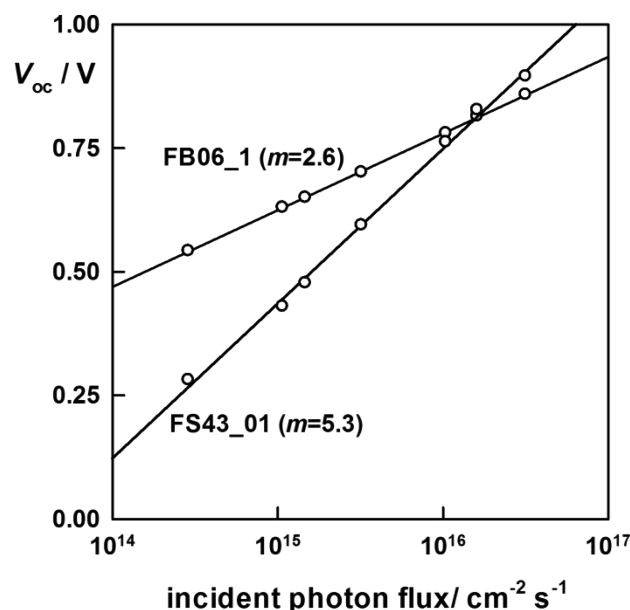


**Figure 2.** Intensity dependence of the open-circuit voltages for two different cells/pixels illustrating the difference in ideality factor between the two groups.

types of intensity dependence of the open-circuit voltage observed when the cells were illuminated with monochromatic light ($\lambda = 625$ nm). Interestingly, the cells fell into two groups. Five of the twelve cells measured showed ideality factors around 2.6 (average = 2.61; std dev = 0.09), and seven showed ideality factors of around 5.2 (average = 5.20; std dev = 0.31). Pixels on the same device always gave similar ideality factors, with three out of the five devices showing higher ideality factors and two showing lower ones.

Interestingly, the cell with the higher ideality factor ($m = 5.3$) gives a higher open-circuit voltage at the highest photon flux ($3.17 \times 10^{16}$ cm$^{-2}$ s$^{-1}$), which in terms of the measured short-circuit currents is equivalent to 0.1 Sun AM 1.5 illumination. However, $V_{oc}$ for this type of cell falls rapidly as the intensity is decreased, so that the plots cross at the equivalent of 0.03 Suns ($1.61 \times 10^{15}$ cm$^{-2}$ s$^{-1}$). The reason for the differences in ideality between two sets of cells made under identical conditions is unknown. We suggest that differences in the annealing temperature due to a small temperature gradient on the hot plate could be responsible. The size and composition of the perovskite crystallites has been shown to be rather dependent on small changes in preparation techniques.[41] In addition, other authors have found two types of behavior for perovskite films that are deposited under identical conditions. Zaban et al.[42] observed two distinct types of behavior for perovskite films sandwiched between gold electrodes; they attributed the differences to the specific structure or orientation of the polycrystalline film with respect to the gold electrodes. We could not find any other literature examples where the ideality factors from $V_{oc}$ versus intensity data for perovskite cells have been reported.

**Open-Circuit Voltage Decay and IMVS.** Experimental OCVD decay plots for the cells are shown in Figure 3. Again, two distinct types of behavior were observed. It can be seen
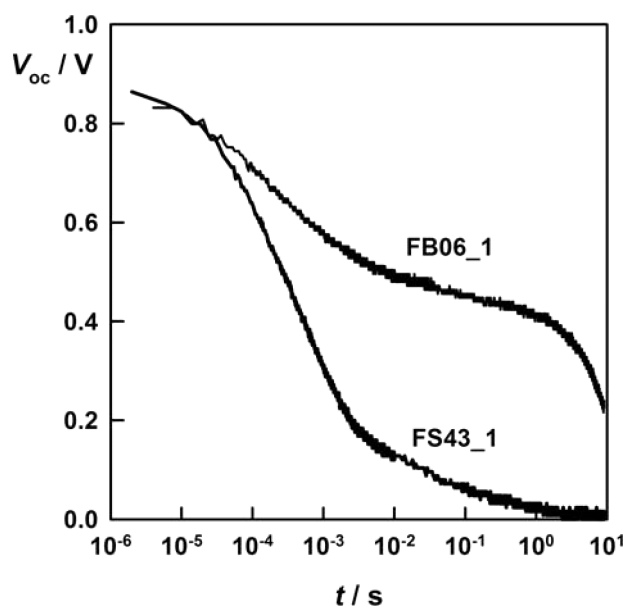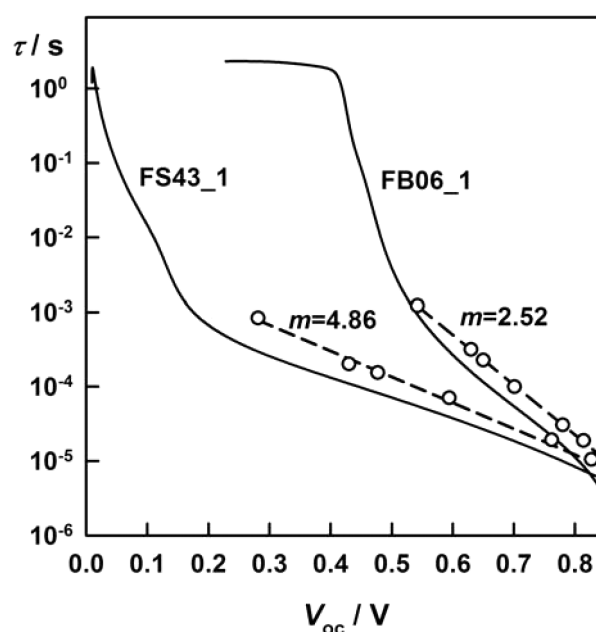
**Figure 3.** Open-circuit voltage decays for the two types of cell. Note that the cell with the lower $m$ value in Figure 2 (FB-06_1) exhibits the anomalously slow voltage decay, whereas the voltage of a cell with $m$ = 5.3 decays much more rapidly.



**Figure 4.** Lifetimes ($\tau_{IMVS}$ and $\tau_{OCVD}$) for the two cells derived from the open-circuit voltage decay (lines) and from the IMVS response (open circles). Regression fits of the IMVS lifetimes give the values of $m$ shown in the figure. These are similar to those derived from the intensity dependence of the $V_{oc}$ (see Figure 2).

that the cell with $m$ = 2.6 in Figure 2 exhibits a remarkably slow decay of $V_{oc}$: the voltage is still 0.4 V after 1 s, and the decay is not complete even at 10 s. By contrast, the open-circuit voltage of the cell with $m$ = 5.3 decays much more rapidly, falling below 0.1 V in only 10 ms. Similar anomalously slow OCVD behavior has been reported by Baumann et al.[25] for vapor-deposited perovskite cells in which the $TiO_2$ and MeOTAD contacts were replaced by $PC_{70}PCBM$ and PEDOT:PSS/polyTPD, respectively. The authors interpreted the decay in terms of the kinetics of electron−hole recombination and found that the recombination order was between 2 and 3 and that it varied depending on the illumination intensity the cell was exposed to prior to the decay.

The IMVS responses (Figure S8, Supporting Information, shows representative IMVS data) of the cells measured over two decades of light intensity were well-defined semicircles in the complex plane, and $\tau_{IMVS}$ was derived from the inverse of the radial frequency corresponding to the maximum of the imaginary component.

The lifetimes derived from the OCVD plots in Figure 3 and from the corresponding IMVS measurements on the two representative cells are presented in Figure 4. Details of the smoothing and fitting procedures used to obtain $\tau_{OCVD}$ are given in the Supporting Information. The reasonable agreement between the lifetimes derived by the transient and small sinusoidal modulation methods indicates that the open-circuit decays through a set of quasistatic states, at least in the voltage range preceding the steeper rise in lifetime that can be seen in the $\tau$ plots for both cells. The slopes of the regression fits of the IMVS plots for the two types of cell correspond to $m$ values, which are similar to those derived from the intensity dependence of the open-circuit voltage (cf. Figure 2). It is important to note that as the geometric capacitance dominates the response of the planar cells (see Supporting Information discussion in the next section), OCVD and IMVS are not measuring the time constant for ambipolar recombination. The

relaxation time, $\tau_{IMVS}/\tau_{OCVD}$, instead appears to be dictated by the product $R_{rec}C_{geo.}$.

The lifetimes measured by IMVS for the two cells were found to be inversely proportional to the incident light intensity as shown in Figure 5. Remarkably, the lifetimes of the two cells at the same light intensity are very similar, in spite of the fact that the open-circuit voltages (and presumably therefore the excess electron and hole concentrations) are quite different. As shown below, the recombination resistances of the two cells measured by impedance spectroscopy were also very similar
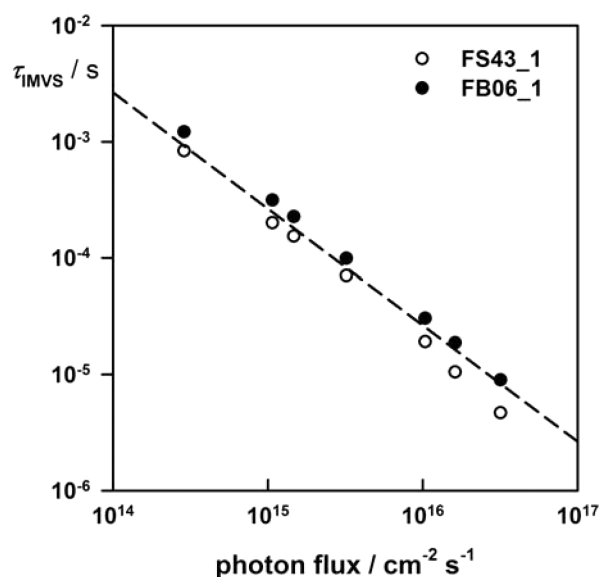


**Figure 5.** Intensity dependence of the lifetimes measured by IMVS for the two cells. The broken line corresponds to a linear dependence (slope = −1).

when measured at the same illumination intensity (cf. Figure 8). The recombination resistance is expected to vary linearly with the inverse of light intensity, providing the dark and light responses from the cell are additive (see Supporting Information). As the lifetime $\tau_{IMVS}/\tau_{OCVD}$ equals $R_{rec}C_{geo}$ in the case of the cells measured here, it follows that $\tau_{IMVS}/\tau_{OCVD}$ should also vary linearly with light intensity provided that $C_{geo}$ is effectively constant across the full range of light intensities measured. This contrasts strongly with the case of normal p−n junctions, where the chemical capacitance is dominant and increases with light intensity due to the increase in electron and hole concentrations.

**Impedance.** Impedance measurements were carried out at open circuit under illumination (and also in the dark as a function of voltage bias, see Supporting Information). Figure 6a
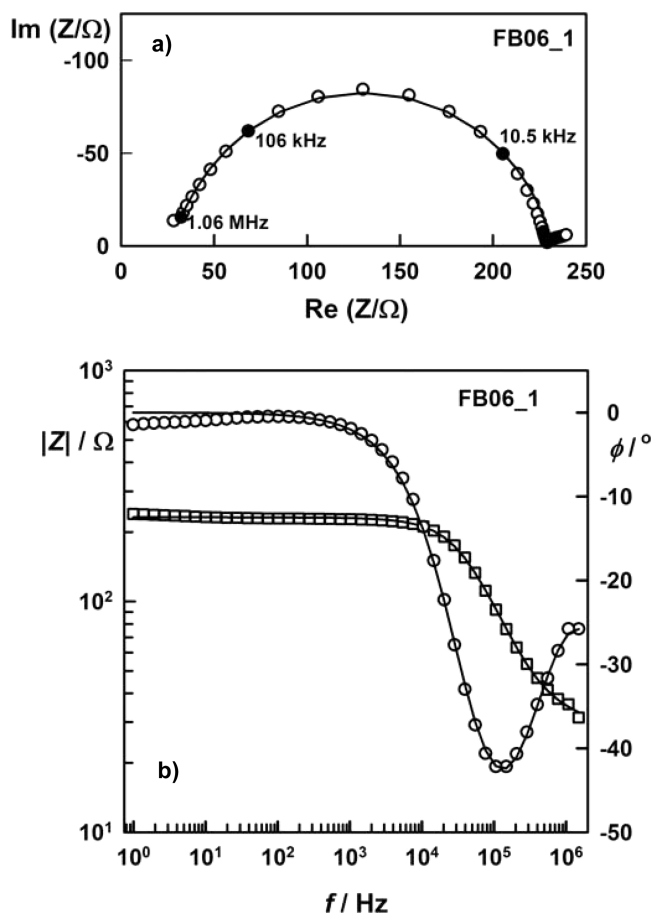


**Figure 6.** (a) Example of the impedance response measured at open circuit at the highest light intensity ($\lambda$ = 625 nm, 3.17 × 10^16 cm^−2 s^−1). Points are the experimental, line fitting to the circuit shown in Figure 1. (b) Bode plot (symbols) and fit (lines) to the circuit shown in Figure 1 with $C_{jun}$ replaced by a constant phase shift element for the impedance response.

and 6b illustrates the impedance response observed at an intensity corresponding to ~0.1 Sun. At all intensities three typical features were seen in the Nyquist plots. A mid-frequency semicircle was attributed to $C_{total}$ and $R_{rec}$. The semicircle was distorted at the highest frequencies by another process which we attributed the effect of stray capacitance (e.g., from the connectors); however, it could also be due to the impedance of the titania blocking layer. A third low-frequency feature was

always observed below ~100 Hz, as illustrated in Figure 6a. Each of the features is discussed in more detail below.

Impedance measurements have been used extensively to characterize mesostructured lead halide perovskite solar cells.[10,22,24] In the case of the mesostructured cells, the analysis has been based on transmission line models developed for dye-sensitized solar cells that consider electron transport and recombination.[10,13,21,26,43] In the case of the planar perovskite cells studied here, we did not observe transmission line behavior, even at the highest frequencies (1.5 MHz). It is likely therefore that for these planar cells the transport of carriers through the perovskite films is too fast to be measured by impedance spectroscopy. This result suggests that the response of these planar cells is much simpler than that of mesostructured cells, and it is possible that the transmission line seen in mesostructured cells is a result of the electrons in the titania scaffold rather than in the perovskite itself.

The time constant for the semicircle obtained in the impedance of all the planar cells, at all illumination intensities, was much shorter than the relaxation time reported for the giant dielectric effect.[12,36,13,26] The response can be fitted to the simple circuit shown in Figure 1 if the total capacitance is replaced by a constant phase shift element. When this was done the $P$ values for the CPE representing $C_{total}$ were all between 0.87 and 1 (see Supporting Information for further discussion). It should also be noted that fitting the mid-frequency range of the semicircle to a simple model containing only $R_{ser}$, $R_{rec}$, and $C_{total}$ without a CPE gave a reasonable fit and showed identical trends in the recombination resistance. When the simple $R_{ser}(R_{rec}C_{total})$ model was used, $C_{total}$ (e.g., reported here for FS43_1) had values of between 20 and 32 nF over the entire intensity (and hence voltage) range. The geometric capacitance for a perfectly smooth device can be calculated to be ~5.3 nF ($C = \varepsilon_0\varepsilon_r A/d$; $A$ = 0.15 cm^2, $d$ = 600 nm, $\varepsilon_r$ = 24[12,44]). The experimentally derived values of the capacitance are approximately 4 times larger than the calculated geometric capacitance for the cell using a relative permittivity of 24. This suggests either a perfectly flat perovskite film with a relative permittivity of 100 or a film with a relative permittivity of 24 and a roughness factor of 4. A roughness factor of 4 is entirely reasonable for a multicrystalline perovskite film; mechanically polished gold films have roughness factors of between 3 and 5, for example.[45] However, the difference in calculated and measured capacitance could also be due to an increase in dielectric constant under illumination as reported by Juarez-Perez et al.[13]

The impedance results strongly suggests that $C_{total}$ is dominated by the value of the geometric capacitance and that the charge stored in the contacts is significantly larger than the charge due to photogenerated electrons and holes in the perovskite. In contrast to measurements on mesostructured cells with titania scaffolds, we do not appear to measure the chemical capacitance and do not see large amounts of charge stored in the bulk of the perovskite.[13,33] Previous measurements on planar perovskite cells (300 nm active layer) also showed a large capacitance which was attributed to a high intrinsic density of states in perovskite films.[21] We did not observe such a large capacitance in our measurements, and the devices studied here show a capacitance which does not vary strongly with intensity. It is possible that the capacitance behavior depends on the methods used to prepare the perovskite cells, as several recent papers have shown large differences in cell properties for small differences in preparation

techniques.[46−48] The fact that $C_g$ dominates $C_\mu$ over the frequency range is consistent with a p−i−n device, although other authors have suggested that perovskite solar cells may function as p−n devices.[49]

The parallel resistance that accompanies $C_{geo}$ is attributed to the recombination resistance. The lifetimes calculated from the product of $C_{geo}$ and $R_{rec}$ agree well with the values measured by IMVS and OCVD (Figure 4 and Figure S9, Supporting Information). We therefore conclude that the perovskite can be considered as essentially intrinsic. This is consistent with the very low doping density (∼$10^9$ cm$^{-3}$) calculated from the transition to first-order decay seen in Figure 4. The variations of the recombination resistance with $V_{oc}$ and with intensity are shown in Figures 7 and 8. The semilogarithmic plots of $R_{rec}$ vs
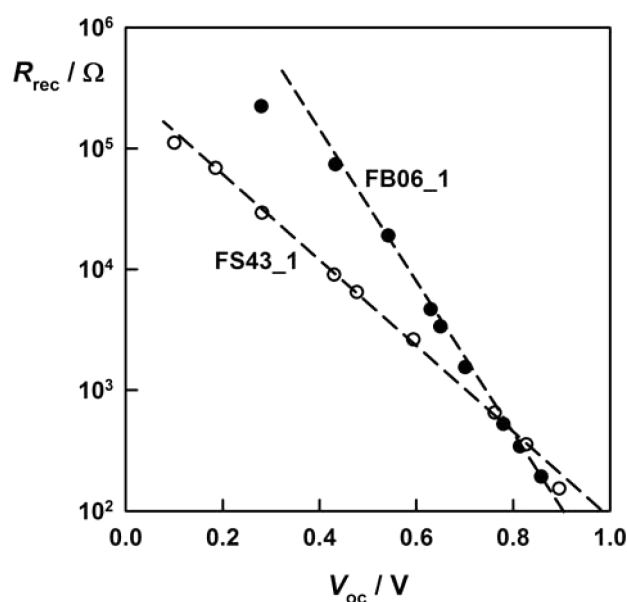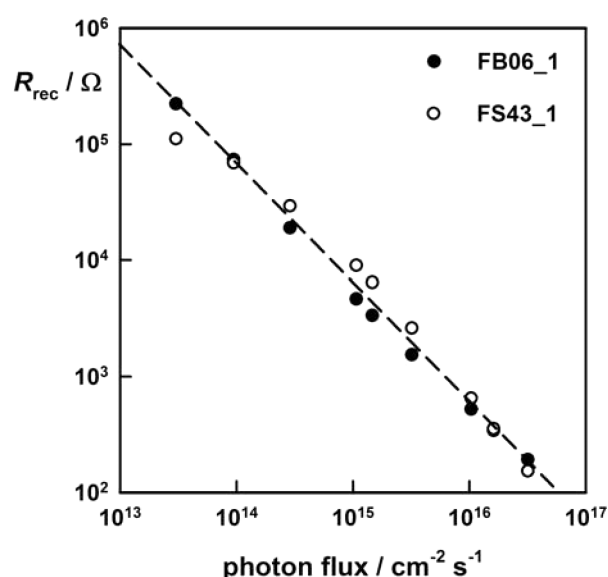


**Figure 7.** Recombination resistance for the two different types of cells measured at open circuit under different illumination intensities. Slopes of the lines shown are 281 mV/decade for FS43-1 and 161 mV/decade for FB-06, corresponding to $m$ values of 4.8 and 2.7, respectively.

$V_{oc}$ for the two types of cells have different slopes as shown in Figure 7, reflecting the different ideality factors of the cells. The ideality factors of 2.7 and 4.8 are very similar to those obtained from the intensity dependence of the open-circuit voltage (cf. Figure 2). By contrast, the intensity dependence of $R_{rec}$ is almost identical for both types of cells, with a slope close to −1, mirroring the intensity dependence of $\tau_{IMVS}$ measured by IMVS (cf. Figure 5).

The low-frequency feature that appears in the impedance plots below 100 Hz has not been studied in detail, as we were concerned that the cells could degrade on the time scale of the very slow low-frequency measurements. Juarez-Perez et al. attribute the low-frequency feature to the GDE in the perovskite.[13] We are currently looking at the low-frequency feature in more detail, but the conclusion of this paper is that a simple circuit gives a good fit to all data above 100 Hz.
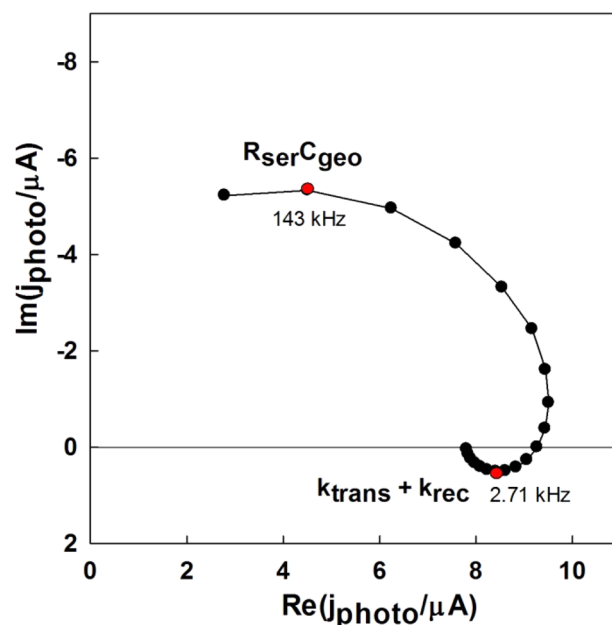
## ■ IMPS

IMPS has been extensively used to investigate carrier transport in DSC. It has also been used to study recombination and interfacial transfer of minority carriers in illuminated semi-



**Figure 8.** Intensity dependence of the recombination resistance for the two cells. The broken line corresponds to a linear dependence of $R_{rec}$ on incident photon flux.

conductor electrodes.[39,40,50] IMPS was recently used by Guillén et al. to study mesostructured perovskite cells; two time constants were observed in one quadrant of the complex plane plot. Figure 9 shows a representative IMPS plot for FS43_1 at



**Figure 9.** IMPS response for FS43_1 showing the RC time constant at high frequency and a low-frequency semicircle which is related to transport and recombination.

0.1 Sun equivalent illumination. The high-frequency semicircle is incomplete as the LED could not be modulated satisfactorily at frequencies higher than 200 kHz. The IMPS response for DSC is usually a semicircle trending to a 45° line toward the origin at high frequencies. The characteristic frequency of the semicircle is related to the electron transport time, which ranges from milliseconds to seconds, depending on the illumination intensity. By contrast, in the case of the planar perovskite solar

cells studied here, the high-frequency semicircle is dominated by the time constant $R_{ser}C_{geo}$ of the cell, and it is difficult to deconvolute the effect of carrier transport because the carrier transit times are similar to or shorter than the $RC$ time constant. However, we believe that the distortion of the semicircle at high frequencies may not be an instrumental artifact but could be due to an additional phase lag associated with transport. The values of the series resistance measured by impedance spectroscopy were used to estimate the capacitance from the relaxation time for the high-frequency semicircle. The series resistance for FB06_1, for example, was ~40 Ω, which gave capacitance values of between 26 and 36 nF. These values are consistent with the values of $C_{total}$ obtained from both IMVS and impedance spectroscopy.

Interestingly, a second semicircle in the lower quadrant is seen at lower frequencies. As discussed above, a similar response is observed for illuminated semiconductor/electrolyte junctions, where the second semicircle is due to the relaxation of the minority carrier concentration at short circuit by charge transfer (with rate $k_{trans}$) and recombination (with rate $k_{rec}$) at the solution–electrode interface. The high-frequency intercept corresponds to the instantaneous photocurrent and the low-frequency limit to the steady-state photocurrent. In this case, the semicircle has a radial frequency at the minimum that is equal to the inverse of the relaxation lifetime, $\tau_{IMPS}^{-1} = k_{trans} + k_{rec}$, and a normalized low-frequency intercept that depends on the charge transfer efficiency, $\eta_{trans} = k_{trans}/(k_{trans} + k_{rec})$. It should be noted that the "relaxation lifetime" measured using IMPS is quite separate from the "recombination lifetime", which is measured at open circuit. The open-circuit recombination lifetime is the product of the chemical capacitance and the recombination resistance. In contrast, the relaxation lifetime from IMPS is measured at short circuit. The IMPS lifetime is not influenced by the geometric capacitance which, as outlined above, is observed in the high-frequency semicircle in the upper quadrant of the IMPS plot. IMPS can therefore give useful information about interfacial charge transport and recombination in perovskite solar cells at short circuit.

In view of the similarity mentioned above, we attribute the low-frequency IMPS response for the perovskite cells to relaxation of photogenerated carriers due to interfacial recombination and transport at short circuit. Values for $k_{trans}$, $k_{rec}$, $\tau_{IMPS}$, and $\eta_{trans}$ were extracted from the maximum frequency and normalized low-frequency intercepts of the IMPS plots recorded as a function of light intensity. Figure 10 shows the collection efficiency, $\eta_{trans}$, for the two cells studied in detail in this paper. It can be seen that $\eta_{trans}$ for FS43_1 is higher than that of FB06_1 at all intensities. This result is consistent with the higher global efficiency measured for this cell.

Figure 11 shows the short-circuit relaxation lifetime calculated from the maximum of the low-frequency IMPS semicircles. A linear variation with intensity is seen for $\tau_{IMPS}$, and its values are higher than the values of $\tau_{IMVS}$ measured at the same light intensities. The calculated rate constants are shown in Figure 12. At all intensities $k_{trans}$ is approximately an order of magnitude greater than $k_{rec}$, which is consistent with the high external quantum efficiencies typically measured for perovskite solar cells under short-circuit conditions. Cell FB06_1 showed a higher recombination rate than cell FS43_1 ($3.43 \times 10^3$ s$^{-1}$ compared to $3.18 \times 10^3$ s$^{-1}$ at 0.1 Sun); the rate constant for interfacial transport was also slower
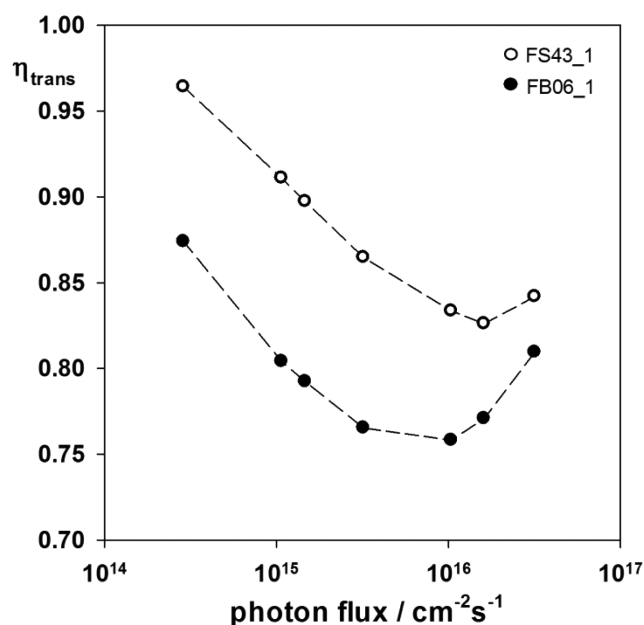


**Figure 10.** Collection efficiency, $\eta_{trans}$, for FB06_1 and FS43_1 calculated from the intercept of the low-frequency semicircle in the IMPS.
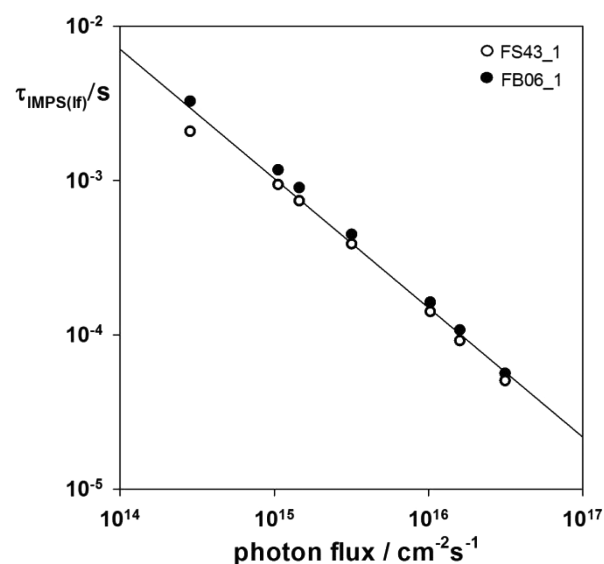


**Figure 11.** $\tau_{IMPS}$ from IMPS measurements of FB06_1 and FS43_1.

($1.46 \times 10^4$ s$^{-1}$ compared to $1.69 \times 10^4$ s$^{-1}$). The differences between the cells increased at lower illumination levels. This data is consistent with the lower short-circuit current observed for FB06_1. The variation in $\eta_{trans}$ with intensity is due to the changes in $k_{trans}$ and $k_{rec}$ with intensity. The data in Figure 11 is not linear with intensity, with $k_{trans}$ increasing and $k_{rec}$ decreasing as the light intensity is decreased.

Further work is in progress to relate the rate constants derived from the IMPS measurements to models of surface recombination.

## ■ CONCLUSIONS

IMVS, OCVD, impedance, and IMPS have been used to study planar perovskite solar cells. Despite the fact that all cells were made at the same time, two distinct sets of behaviors were seen. One half of the cells had ideality factors of ~2.6, and the other
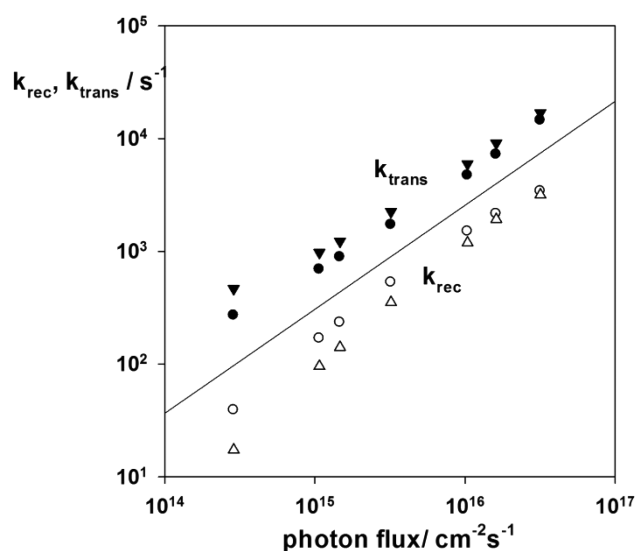
**Figure 12.** Recombination rate constant (open symbols) and transport rate constant (solid symbols) as a function of intensity. Circles show data for FB06_1, and triangles show data for FS43_1.

half showed ideality factors of ~5.2. The difference in behavior was also seen in the OCVD: the cells with the lower ideality factors showed a persistent photovoltage. Lifetimes from IMVS were in good agreement with those calculated from OCVD. IMVS and impedance spectroscopy showed time constants that were dominated by the geometric capacitance rather than the chemical capacitance, meaning that the ambipolar recombination lifetime could not be extracted. IMPS showed two semicircles, one at high frequency attributed to the RC time constant of the cells and a second at lower frequency attributed to interfacial transport and recombination at short circuit. Analysis of the IMPS response suggests that the collection of photogenerated carriers is very efficient under short-circuit conditions in these planar perovskite cells

### ■ ASSOCIATED CONTENT

#### ⓢ Supporting Information
IV characteristics and cell efficiencies, IMVS results, analysis of constant phase shift elements, dark impedance, OCVD fitting and theory, and modeling of the geometric and chemical capacitance for a planar p–i–n cell. This material is available free of charge via the Internet at http://pubs.acs.org.

### ■ AUTHOR INFORMATION

**Corresponding Authors**
*E-mail: l.m.peter@bath.ac.uk.
*E-mail: p.j.cameron@bath.ac.uk.

**Author Contributions**
The manuscript was written through contributions of all authors. All authors have given approval to the final version of the manuscript.

**Notes**
The authors declare no competing financial interest.

### ■ ACKNOWLEDGMENTS

### ■ REFERENCES

(1) Liu, M.; Johnston, M. B.; Snaith, H. J. Efficient Planar Heterojunction Perovskite Solar Cells by Vapour Deposition. *Nature* **2013**, *501*, 395−398.

(2) Lee, M. M.; Teuscher, J.; Miyasaka, T.; Murakami, T. N.; Snaith, H. J. Efficient Hybrid Solar Cells Based on Meso-Superstructured Organometal Halide Perovskites. *Science* **2012**, *338*, 643−647.

(3) Etgar, L.; Gao, P.; Xue, Z.; Peng, Q.; Chandiran, A. K.; Liu, B.; Nazeeruddin, M. K.; Grätzel, M. Mesoscopic $CH_3NH_3PbI_3$/$TiO_2$ Heterojunction Solar Cells. *J. Am. Chem. Soc.* **2012**, *134*, 17396−17399.

(4) Kim, H.-S.; Lee, C.-R.; Im, J.-H.; Lee, K.-B.; Moehl, T.; Marchioro, A.; Moon, S.-J.; Humphry-Baker, R.; Yum, J.-H.; Moser, J. E.; et al. Lead Iodide Perovskite Sensitized All-Solid-State Submicron Thin Film Mesoscopic Solar Cell with Efficiency Exceeding 9%. *Sci. Rep.* **2012**, *2*, 591.

(5) Bretschneider, S. A.; Weickert, J.; Dorman, J. A.; Schmidt-Mende, L. Research Update: Physical and Electrical Characteristics of Lead Halide Perovskites for Solar Cell Applications. *APL Mater.* **2014**, *2*, 040701.

(6) Ryu, S.; Noh, J. H.; Jeon, N. J.; Kim, Y. C.; Yang, W. S.; Seo, J. W.; Seok, S. I. Voltage Output of Efficient Perovskite Solar Cells with High Open-Circuit Voltage and Fill Factor. *Energy Environ. Sci.* **2014**, *7*, 2614−2618.

(7) Wehrenfennig, C.; Eperon, G. E.; Johnston, M. B.; Snaith, H. J.; Herz, L. M. High Charge Carrier Mobilities and Lifetimes in Organolead Trihalide Perovskites. *Adv. Mater.* **2014**, *26*, 1584−1589.

(8) Yin, W.-J.; Shi, T.; Yan, Y. Unique Properties of Halide Perovskites as Possible Origins of the Superior Solar Cell Performance. *Adv. Mater.* **2014**, *26*, 4653−4658.

(9) Ponseca, C. S.; Savenije, T. J.; Abdellah, M. A.; Zheng, K.; Yartsev, A. P.; Pascher, T.; Harlang, T.; Chabera, P.; Pullerits, T.; Stepanov, A.; et al. Organometal Halide Perovskite Solar Cell Materials Rationalized−Ultrafast Charge Generation, High and Microsecond-Long Balanced Mobilities and Slow Recombination. *J. Am. Chem. Soc.* **2014**, *136*, 5189−5192.

(10) Gonzalez-Pedro, V.; Juarez-Perez, E. J.; Arsyad, W.-S.; Barea, E. M.; Fabregat-Santiago, F.; Mora-Sero, I.; Bisquert, J. General Working Principles of $CH_3NH_3PbX_3$ Perovskite Solar Cells. *Nano Lett.* **2014**, *14*, 888−893.

(11) Frost, J. M.; Butler, K. T.; Brivio, F.; Hendon, C. H.; van Schilfgaarde, M.; Walsh, A. Atomistic Origins of High-Performance in Hybrid Halide Perovskite Solar Cells. *Nano Lett.* **2014**, *14*, 2584−2590.

(12) Frost, J. M.; Butler, K. T.; Walsh, A. Molecular Ferroelectric Contributions to Anomalous Hysteresis in Hybrid Perovskite Solar Cells. *APL Mater.* **2014**, *2*, 081506.

(13) Juárez-Pérez, E. J.; Sánchez, R. S.; Badia, L.; Garcia-Belmonte, G.; Kang, Y. S.; Mora-Sero, I.; Bisquert, J. Photoinduced Giant Dielectric Constant in Lead Halide Perovskite Solar Cells. *J. Phys. Chem. Lett.* **2014**, *9*, 2390−2394.

(14) Zhou, H.; Chen, Q.; Li, G.; Luo, S.; Song, T.-b.; Duan, H.-S.; Hong, Z.; You, J.; Liu, Y.; Yang, Y. Interface Engineering of Highly Efficient Perovskite Solar Cells. *Science* **2014**, *345*, 542−546.

(15) Savenije, T. J.; Ponseca, C. S.; Kunneman, L. T.; Abdellah, M. A.; Zheng, K.; Tian, Y.; Zhu, Q.; Canton, S. E.; Scheblykin, I. G.; Pullerits, T.; et al. Thermally Activated Exciton Dissociation and Recombination Control the Organometal Halide Perovskite Carrier Dynamics. *J. Phys. Chem. Lett.* **2014**, *5*, 2189−2194.

(16) Marchioro, A.; Teuscher, J.; Friedrich, D.; Kunst, M.; van de Krol, R.; Moehl, T.; Grätzel, M.; Moser, J.-E. Unravelling the Mechanism of Photoinduced Charge Transfer Processes in Lead Iodide Perovskite Solar Cells. *Nat. Photonics* **2014**, *8*, 1−6.

(17) Wehrenfennig, C.; Liu, M.; Snaith, H. J.; Johnston, M. B.; Herz, I. Charge-Carrier Dynamics in Vapour-Deposited Films of the Organolead Halide Perovskite $CH_3NH_3PbI_3-xClx$. *Energy Environ. Sci.* **2014**, 2269−2275.

(18) Stranks, S. D.; Eperon, G. E.; Grancini, G.; Menelaou, C.; Alcocer, M. J. P.; Leijtens, T.; Herz, L. M.; Petrozza, A.; Snaith, H. J. Electron-Hole Diffusion Lengths Exceeding 1 Micrometer in an Organometal Trihalide Perovskite Absorber. *Science* **2013**, *342*, 341−344.

(19) Edri, E.; Kirmayer, S.; Henning, A.; Mukhopadhyay, S.; Gartsman, K.; Rosenwaks, Y.; Hodes, G.; Cahen, D. Why Lead Methylammonium Tri-Iodide Perovskite-Based Solar Cells Require a Mesoporous Electron Transporting Scaffold (but Not Necessarily a Hole Conductor). *Nano Lett.* **2014**, *14*, 1000−1004.

(20) Abate, A.; Saliba, M.; Hollman, D. J.; Stranks, S. D.; Wojciechowski, K.; Avolio, R.; Grancini, G.; Petrozza, A.; Snaith, H. J. Supramolecular Halogen Bond Passivation of Organic-Inorganic Halide Perovskite Solar Cells. *Nano Lett.* **2014**, 3247−3254.

(21) Kim, H.-S.; Mora-Sero, I.; Gonzalez-Pedro, V.; Fabregat-Santiago, F.; Juarez-Perez, E. J.; Park, N.-G.; Bisquert, J. Mechanism of Carrier Accumulation in Perovskite Thin-Absorber Solar Cells. *Nat. Commun.* **2013**, *4*, 2242.

(22) Dualeh, A.; Moehl, T.; Tétreault, N.; Teuscher, J.; Gao, P.; Nazeeruddin, M. K.; Grätzel, M. Impedance Spectroscopic Analysis of Lead Iodide Perovskite-Sensitized Solid-State Solar Cells. *ACS Nano* **2014**, *8*, 362−373.

(23) Sanchez, R. S.; Gonzalez-Pedro, V.; Lee, J.-W.; Park, N.-G.; Kang, Y. S.; Mora-Sero, I.; Bisquert, J. Slow Dynamic Processes in Lead Halide Perovskite Solar Cells. Characteristic Times and Hysteresis. *J. Phys. Chem. Lett.* **2014**, *5*, 2357−2363.

(24) Suarez, B.; Gonzalez-Pedro, V.; Ripolles, T. S.; Sánchez, R. S.; Otero, L. A.; Mora-Sero, I. Recombination Study of Combined Halides (Cl, Br, I) Perovskite Solar Cells. *J. Phys. Chem. Lett.* **2014**, *5*, 1628−1635.

(25) Baumann, A.; Tvingstedt, K.; Heiber, M. C.; Väth, S.; Momblona, C.; Bolink, H. J.; Dyakonov, V. Persistent Photovoltage in Methylammonium Lead Iodide Perovskite Solar Cells. *APL Mater.* **2014**, *2*, 081501.

(26) Bisquert, J.; Bertoluzzi, L.; Mora-Sero, I.; Garcia-Belmonte, G. Theory of Impedance and Capacitance Spectroscopy of Solar Cells with Dielectric Relaxation, Drift-Diffusion Transport, and Recombination. *J. Phys. Chem. C* **2014**, *118*, 18983−18991.

(27) Landsberg, P. T. *Recombination in Semiconductors*; Cambridge University Press: Cambridge, U.K., 1991.

(28) Shah, J. M.; Li, Y.-L.; Gessmann, T.; Schubert, E. F. Experimental Analysis and Theoretical Model for Anomalously High Ideality Factors ($N \gg 2.0$) in AlGaN/GaN P-N Junction Diodes. *J. Appl. Phys.* **2003**, *94*, 2627−2630.

(29) Brug, G. J.; van den Eeden, A. L. G.; Sluyters-Rehbach, M.; Sluyters, J. H. The Analysis of Electrode Impedances Complicated by the Presence of a Constant Phase Element. *J. Electroanal. Chem. Interfacial* **1984**, *176*, 275−295.

(30) Hirschorn, B.; Orazem, M. E.; Tribollet, B.; Vivier, V.; Frateur, I.; Musiani, M. Constant-Phase-Element Behavior Caused by Resistivity Distributions in Films. In *Corrosion*; Hansen, D. C., Alfantazi, A., Gelling, V. J., Eds.; The Electrochemical Society: New Jersey, 2010; Vol. *28*, pp 77−94.

(31) Mora-Sero, I.; Garcia-Belmonte, G.; Boix, P. P.; Vazquez, M. A.; Bisquert, J. Impedance Spectroscopy Characterisation of Highly Efficient Silicon Solar Cells under Different Light Illumination Intensities. *Energy Environ. Sci.* **2009**, *2*, 678−686.

(32) Bisquert, J. Theory of the Impedance of Electron Diffusion and Recombination in a Thin Layer. *J. Phys. Chem. B* **2001**, *106*, 325−333.

(33) Guillén, E.; Ramos, F. J.; Anta, J. A.; Ahmad, S. Elucidating Transport-Recombination Mechanisms in Perovskite Solar Cells by Small-Perturbation Techniques. *J. Phys. Chem. C* **2014**, *118*, 22913−22922.

(34) Zhao, Y.; Nardes, A. M.; Zhu, K. Mesoporous Perovskite Solar Cells: Material Composition, Charge-Carrier Dynamics, and Device Characteristics. *Faraday Discuss.* **2014**, Advance article. http://dx.doi.org/10.1039/C4FD00128A.

(35) Zhao, Y.; Nardes, A. M.; Zhu, K. Solid-State Mesostructured Perovskite $CH_3NH_3PbI_3$ Solar Cells: Charge Transport, Recombination, and Diffusion Length. *J. Phys. Chem. Lett.* **2014**, *5*, 490−494.

(36) Zaban, A.; Greenshtein, M.; Bisquert, J. Determination of the Electron Lifetime in Nanocrystalline Dye Solar Cells by Open-Circuit Voltage Decay Measurements. *ChemPhysChem* **2003**, *4*, 859−864.

(37) Franco, G.; Peter, L. M.; Ponomarev, E. A. Detection of Inhomogeneous Dye Distribution in Dye Sensitised Nanocrystalline Solar Cells by Intensity Modulated Photocurrent Spectroscopy (IMPS). *Electrochem. Commun.* **1999**, *1*, 61−64.

(38) Ponomarev, E. A.; Peter, L. M. A Generalized Theory of Intensity Modulated Photocurrent Spectroscopy (IMPS). *J. Electroanal. Chem.* **1995**, *396*, 219−226.

(39) Peter, L. M.; Ponomarev, E. A.; Fermín, D. J. Intensity-Modulated Photocurrent Spectroscopy: Reconciliation of Phenomenological Analysis with Multistep Electron Transfer Mechanisms. *J. Electroanal. Chem.* **1997**, *427*, 79−96.

(40) Peter, L. M.; Wijayantha, K. G. U.; Tahir, A. A. Kinetics of Light-Driven Oxygen Evolution at alpha-$Fe_2O_3$ Electrodes. *Faraday Discuss.* **2012**, *155*, 309−322.

(41) Grancini, G.; Marras, S.; Prato, M.; Giannini, C.; Quarti, C.; De Angelis, F.; De Bastiani, M.; Eperon, G. E.; Snaith, H. J.; Manna, L.; et al. The Impact of the Crystallization Processes on the Structural and Optical Properties of Hybrid Perovskite Films for Photovoltaics. *J. Phys. Chem. Lett.* **2014**, *5*, 3836−3842.

(42) Gottesman, R.; Haltzi, E.; Gouda, L.; Tirosh, S.; Bouhadana, Y.; Zaban, A.; Mosconi, E.; De Angelis, F. Extremely Slow Photoconductivity Response of CH3NH3PbI3 Perovskites Suggesting Structural Changes under Working Conditions. *J. Phys. Chem. Lett.* **2014**, *5*, 2662−2669.

(43) Bertoluzzi, L.; Boix, P. P.; Mora-Sero, I.; Bisquert, J. Theory of Impedance Spectroscopy of Ambipolar Solar Cells with Trap-Mediated Recombination. *J. Phys. Chem. C* **2013**, *118*, 16574−16580.

(44) Brivio, F.; Walker, A. B.; Walsh, A. Structural and Electronic Properties of Hybrid Perovskites for High-Efficiency Thin-Film Photovoltaics from First-Principles. *APL Mater.* **2013**, *1*, 042111.

(45) Douglass, E. F., Jr; Driscoll, P. F.; Liu, D.; Burnham, N. A.; Lambert, C. R.; McGimpsey, W. G. Effect of Electrode Roughness on the Capacitive Behavior of Self-Assembled Monolayers. *Anal. Chem.* **2008**, *80*, 7670−7677.

(46) Im, J.-H.; Kim, H.-S.; Park, N.-G. Morphology-Photovoltaic Property Correlation in Perovskite Solar Cells: One-Step Versus Two-Step Deposition of $CH_3NH_3PbI_3$. *APL Mater.* **2014**, *2*, 081510.

(47) Bass, K. K.; McAnally, R. E.; Zhou, S.; Djurovich, P. I.; Thompson, M. E.; Melot, B. C. Influence of Moisture on the Preparation, Crystal Structure, and Photophysical Properties of Organohalide Perovskites. *Chem. Commun.* **2014**, *50*, 15819−15822.

(48) Buin, A.; Pietsch, P.; Xu, J.; Voznyy, O.; Ip, A. H.; Comin, R.; Sargent, E. H. Materials Processing Routes to Trap-Free Halide Perovskites. *Nano Lett.* **2014**, *14*, 6281−6286.

(49) Guerrero, A.; Juarez-Perez, E. J.; Bisquert, J.; Mora-Sero, I.; Garcia-Belmonte, G. Electrical Field Profile and Doping in Planar Lead Halide Perovskite Solar Cells. *Appl. Phys. Lett.* **2014**, *105*, 133902.

(50) Peter, L. M. Dynamic Aspects of Semiconductor Photoelectrochemistry. *Chem. Rev.* **1990**, *90*, 753−769.